Degradation of Encapsulated Perovskite Solar Cells Driven by Deep Trap States and Interfacial Deterioration

Dhruba B. Khadka†‡*, Yasuhiro Shirai†*, Masatoshi Yanagida† and Kenjiro Miyano†

†Global Research Center for Environment and Energy based on Nanomaterials Science (GREEN), National Institute for Materials Science (NIMS), 1-1 Namiki, Tsukuba, Ibaraki 305-0044, Japan.

‡ International Center for Young Scientists (ICYS), National Institute for Materials Science (NIMS), 1-1 Namiki, Tsukuba, Ibaraki 305-0044, Japan.

Corresponding Author

*E-mail:

KHADKA.B.Dhruba@nims.go.jp

SHIRAI.Yasuhiro@nims.go.jp

ABSTRACT

The degradation of encapsulated perovskite device has been investigated by optoelectronic characterizations. The performance of encapsulated device dropped by approximately 50% of initial value after five months. The degradation of device performance was found to be influenced by both interface recombination and deep trap assisted recombination in the perovskite. The analysis of temperature dependent current-voltage characteristics and capacitance spectra revealed that the decrease in activation energy of interface recombination, deepening of the defect levels and reducing diffusion potential of devices led to deterioration of device parameters with aging. The degradation of the encapsulated device might be governed by dissociation and migration of constituent ions which induces deeper defect level in perovskite layer and deteriorates the interface with aging.

Keywords: Perovskite, interfacial recombination, degradation, defect state.

1. Introduction

Perovskite solar cells (PSCs) have drawn enormous attention due to their rapid progress in device efficiencies ~22% showing a competitive performance to silicon and chalcopyrite based photovoltaic devices.[1–3] Although perovskite devices demonstrated startling performance by adopting various fabrication methods[3–7] and device architectures with a number of carrier transport materials (CTMs),[8–10] the poor stability of device has been most problematic for commercialization.[3,11–14] Indeed, the improvement in device stability has been attempted in terms of device structures,[15,16] engineering CTMs,[8,17,18] electrode[11] and coating with hydrophobic materials.[19,20] The degradation of PSCs is reported to be accelerated by external factors such as humidity,[15,21,22] UV light,[23,24] temperature[21,22] and oxygen[21] coupled with intrinsic properties of perovskite materials;[21,25,26] chemical instability, ion migration, dissociation of constituents and worsening of carrier transport layer (CTL) and external contacts.[21,22,27,28] Identifying the mechanisms behind the degradation is crucial to resolve a big hurdle of short lifespan of perovskite devices.

Let us go into some details of the degradation studies quoted above. The atmospheric moisture has been regarded as the main cause for irreversible degradation of perovskite material.[13,21,29,30] Yang et al. investigated the degradation mechanism in controlled humidity using in situ techniques.[31] They observed a rapid degradation of perovskite film under higher humidity and formation of new hydrated compound. Choi and co-workers[32] reported that the moisture induced irreversible degradation of perovskite material is triggered by trapped charges at grain boundaries. In addition, they also observed the synergetic effect of oxygen on degradation. Note that degradation of perovskite film may be influenced by the carrier transport layers[8,17] and contact electrode[11,33], which could make the study of separate perovskite films insufficient. A study by Bryant et al. found that light and oxygen-induced degradation causes the low operational stability of perovskite device exposed to ambient conditions.[34] They

suggested that the operational stability can be critically improved by protecting perovskite with oxygen-impermeable interlayer. Although the device stability improved for encapsulated devices[22,24] or devices kept in nitrogen atmosphere,[3,28,33] they also suffered signification degradation with aging. It indicates that there are intrinsic factors for degradation of perovskite device induced with aging. Cheng and co-workers carried out a post-mortem analysis of encapsulated perovskite devices (significantly degraded) after prolong aging at high temperature and humidity.[22] They observed less severe and slow degradation but the perovskite still decomposes into HI and CH_3NH_2 gases. It is found that the saturated release gases cause voids at interface and corrode the metal contact leading to the device parameter deterioration. Guerrero et al. also reported that interfacial deterioration caused by reaction between metal electrode and perovskite could result in degradation of device in the absence of moisture.[28] Interestingly, Besleaga et al. suggested that iodine is dislocated by electric field between electrodes which causes iodine migration.[33] This results in intrinsic degradation of device. A recent study by Zhang et al. reported that the ion migration accelerated degradation of PSCs at the device level.[27] They observed not only diffusion of mobile iodide from perovskite into CTLs and contact electrode but also diffusion of electrode metal atom/ions into the perovskite. Song et al. suggested that increased trap states at the surface of perovskite induced the performance degradation of PSCs, based on the J-V characteristics and open circuit voltage decay measurements.[35] Moreover, theoretical studies postulated that the interfacial ionic migration and formation of defects such as antisites (MA_{Pb}, $Pb_{MA,}$ $MA_{I,}$ $Pb_{I,}$ I_{Pb}), interstitial (MA_i, Pb_i, X_i) and vacancies (V_{MA}, V_{Pb}, V_I) can deteriorate the optoelectronic quality of perovskite layer and also induce interface degradation leading to dominant effect in device performance.[36–38] Therefore, systematic studies are necessary to correlate the degradation of device performance to the perovskite material properties; chemical decomposition, ionic migration, optophysical/optoelectronic properties, and interfacial interactions.

In this study, we have investigated the degradation of encapsulated devices focusing on optoelectronic characterizations; photocurrent-voltage characteristics and admittance spectra. The degradation of device performance was found to be dominated by interface recombination (decrease in E_A~ 1.40 eV to $\leq$1 eV) and formation of deeper defect states (~0.3 to 0.8 eV). The device simulations were also carried out using SCAPS (solar cell capacitor simulator). The degraded device characteristics were reproduced by adjusting the simulation parameters according to the optoelectronic measurements, which supports our interpretation.

2. Experimental section

Materials and preparation: All chemicals were purchased from commercial suppliers as mentioned and unless otherwise specified, they were used as received. Methylammonium iodide (MAI) and Methylammonium chloride (MACl) were of battery grade from Wako chemical company. PbI_2-DMSO complex was prepared following the report by Seok and co-workers.[39] In brief, PbI_2 (50g) was dissolved in DMSO (150 ml, 60 ℃). After that toluene (350 ml) was slowly added into the PbI_2 solution and the precipitation (PbI_2-$(DMSO)_2$) was filtered and dried for 3 h at room temperature. The PbI_2-$(DMSO)_2$ complex was reduced to PbI_2-DMSO by further annealing the precipitation for 24 h in vacuum oven at 60 ℃. For the fabrication of perovskite films, precursor solution were prepared by dissolving PbI_2- DMSO complex and methylammonium iodide (MAI) + methylammonium chloride (MACl) in anhydrous DMF (500 mg ml^{-1}) and ethanol (50 mg ml^{-1}; 19:1 ratio, by mass), respectively. [6,6]-Phenyl C_{61} butyric acid methyl ester ($PC_{61}BM$) [Sigma Aldrich, 99% purity] solution (2 wt. %) dissolved in anhydrous chlorobenzene (CB) was used for coating of the electron transport layer (ETL). Tetrabutylamonium iodide (TBAI) (Sigma Aldrich, 99% purity) precursor solution (0.01 wt. %) was prepared by dissolving in ethanol for doping of PCBM surface.[40] All the

solutions were filtered using 0.45 μm syringe filters to avoid the risk of unwanted particles in the precursor solution.

Device fabrication: We employed low temperature solution process method to fabricate the planar heterojunction PSCs. First, the ITO substrates were pre-cleaned in an ultrasonic bath with detergent, pure water, and 2-propanol, followed by an ultraviolet-ozone treatment for 5 min to remove the organic residues. A thin HTM layer (30 nm) of poly(3,4-ethylenedioxythiophene):poly(styrene sulfonate) (PEDOT:PSS, Clevios, Al4083) was deposited by spin coating at 3000 rpm and subsequently dried at 130 ℃ for 10 min on a hot plate in air. Then substrates were transferred into a nitrogen-filled glove box (<1.0 ppm O_2 and H_2O) and the rest of the steps were carried out inside the glove box. PbI_2 precursor solution was spin coated at 3000 rpm for 90 s and a mixed precursor solution of MAI + MACl was subsequently spun on to the PbI_2 layer at 4000 rpm, for 30s. Then those as-grown $CH_3NH_3PbI_{3-x}Cl_x$ perovskite films were crystallized simply by placing on a hot plate either with MACl powder in a Petri dish or without MACl powder at 100 ℃. For ETM layer, $PC_{61}BM$ was deposited on top of the perovskite films at 700 rpm for 30 s and subsequently at 5000 rpm for 10 s, followed by deposition of a thin TBAI layer spun at 3000 rpm for 25 s. Note that the device fabricated with MACl treatment is denoted as device-I and that of without MACl treatment is device-II. To complete device structure, those samples were then transferred into the evaporation chamber connected to the glove box for metal contact deposition. 100 nm of Ag was thermally evaporated at a base pressure $<10^{-4}$ Pa and get complete devices with area of ~0.26 cm^2. Then, all devices were sealed using UV-curable resin (UV RESIN XNR5516Z; Nagase ChemeteX, Japan) inside the glove box before the subsequent measurements in ambient conditions. For encapsulation, the perovskite device was covered with transparent plastics well fitted to device size which was glued using UV-curable resin. The device encapsulation was completed by baking the sealed device under UV-light for 5 min.

Device characterizations: The current density–voltage (J-V) characteristics and spectral responses (external quantum efficiency (EQE), internal quantum efficiency (IQE) and reflectance spectra) were characterized with a spectrometer (SM-250, RU-60 with integrated sphere, Bunko Keiki, Japan). Capacitance-frequency (C-f) response was measured with an LCR meter (E4980A, Agilent), which probes from 20 Hz to 2 MHz at ac voltage amplitude of 10 mV under dark condition in the temperature range of 253K−343K whereas capacitance-voltage (C−V) measurements were carried out at 1kHz. For temperature dependent characterizations, we used a temperature controlled chamber (SU-221) having control error of ±0.1K (℃).

3. Results and discussion

We chose two types of encapsulated perovskite solar cells (PSCs) of device structure ITO/PEDOT:PSS/perovskite/ PCBM/TBAI/Ag (**Fig. S1**); (a) device-I having the best PCE in the range; η~14-15% and (b) device-II having the best PECE in the range; η=11-12%. As stated earlier, device-I was fabricated with MACl treatment and device-II without. The details of device characterizations have been discussed in our previous report.[6] Two types of devices (better and lower initial quality, respectively) were intentionally chosen in order to see if the mode of degradation depends on the initial quality. The difference between the two was presumed to be due to the bulk crystallinity of the perovskite layer. We analysed the J-V characteristics and capacitance spectroscopy of fresh and degraded devices.

3.1. Device degradation and electrical properties

Figure 1a depicts the J-V curves of encapsulated perovskite devices degraded with aging. Those devices were stored under ambient conditions and measured periodically under standard conditions, one sun illumination, AM 1.5G at room temperature. The device parameters are

summarized in **Table 1.** We observed a noticeable drop on open circuit voltage (V_{OC}) rather than short circuit current (J_{SC}) during the first three months. The performance of our devices dropped by approximately fifty percent of initial PCE after five months. The perovskite devices without encapsulation degrade much faster due to various external factors.[21,22,35] The degradation trends of device parameters with aging have been summarized in supporting information (**Fig. S2, Table S1**). Note that we tested J-V characteristics (**Fig. S3**) of encapsulated device under standard testing condition (one sun illumination, AM 1.5G) by varying relative humidity (30%-90%) for confirmation of encapsulation. No noticeable variation was observed in figures of merit of device even in severely humid environment. It indicates that internal factors are the primary cause for degradation. Multiple reports suggested that ion migration in device results in interfacial worsening and deterioration of perovskite layer which accelerates degradation.[27,28,33].

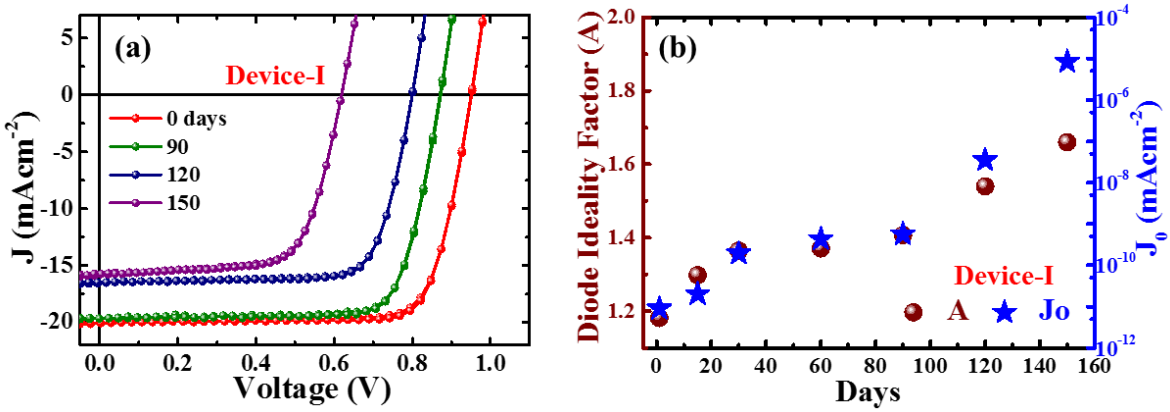

Fig. 1. J-V characteristics of the perovskite solar cells (device-I) after different aging time interval (a). Diode ideality factor (A) and reverse saturation current density (J_0) (b) of the perovskite devices extracted from analysis of respective J-V curves.

Table 1. Photovoltaic parameters of devices after various aging period.

Devices perforamnce / days	Device-I			
	J_{SC} ($mAcm^{-2}$)	V_{OC} (V)	FF (%)	η (%)
0	20.12	0.95	79.81	15.09
90	19.93	0.89	78.47	13.33
120	16.48	0.79	76.79	10.12
150	15.56	0.62	70.15	6.71

To understand the degradation kinetics of the perovskite devices, we extracted the electrical parameters; diode ideality factor (A) and reverse saturation current density (J_0) which are related to defect activities in the devices,[41–43] by fitting with the diode equation.[43]

$$J(V) = J_0 \left[exp\left(\frac{q(V-R_S J)}{Ak_B T}\right) - 1 \right] + \frac{V-R_S J}{R_{Sh}} - J_{Ph}(V) \qquad (1)$$

Where R_S and R_{Sh} are series and shunt resistance of the devices, J_{Ph} photocurrent and k_B the Boltzmann constant. The estimated parameters are listed in **Table S1** for fresh and degraded devices. As shown in **Fig. 1b**, the parameters (A, J_0) increase with the degradation, which agree with the reported values[35]: A increased from ~1.1 for a fresh device to ~1.7 for a degraded device and J_0 increased from ~9.03×10^{-12} $mAcm^{-2}$ to 8.46×10^{-6} $mAcm^{-2}$ for respective devices. Note that we observed pretty much parallel degradation trend for device-II with slightly higher values of A and J_0 as summarized in supporting information (**Fig. S2, Fig. S4, Table S1**). Our further analysis of aging effects also revealed similar characteristic trends for both devices indicating same origin of degradation phenomena, which turned out to be insensitive to the crystallinity of the perovskite layer. Hence, we consider characteristic trend of device-I on further analysis and discussion hereafter.

The spectral response change with aging (**Fig. S5**) revealed a significant loss in EQE in the range of 300-730 nm that indicates inefficient carrier collection. It is attributed to the degradation of perovskite layer and deterioration of interfacial carrier transport layer. [43,44] The higher values of A and J_0 with aging signify that the degradation of device performances is attributed to increasing trap assisted recombination phenomena.[41–43] This could be due to either intrinsic instability of perovskite material, ill-behaved interface at CTLs, or intra-layer ion migration in perovskite device.[22,27,28] We will discuss some of them below.

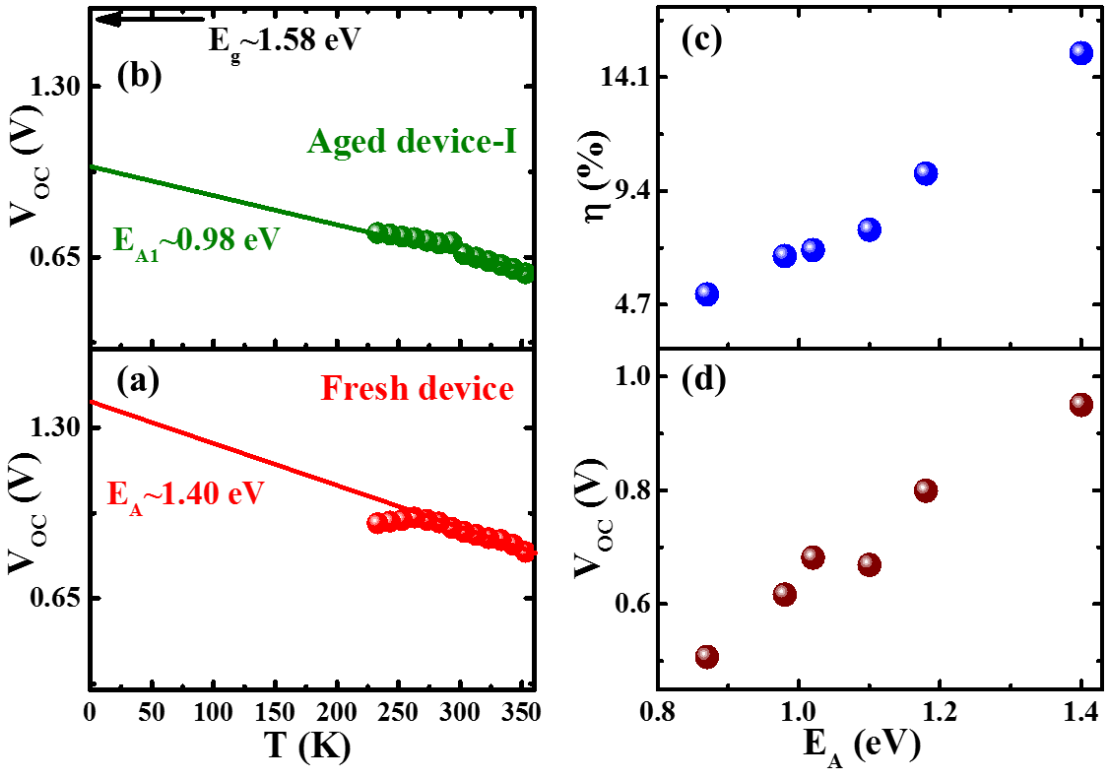

Fig. 2. The temperature dependent open circuit voltage (V_{OC}-T) of fresh device (a) and degraded device (b). Plots of trend of efficiency (η) (c) and V_{OC} (d) of fresh and aged devices with activation energy of interface recombination (E_A).

To investigate the impact of aging on interface layer quality and recombination mechanism, the temperature dependent J-V characteristics were studied in the temperature range 233 to 353 K. The temperature range was chosen to avoid the phase transition of

perovskite crystal.[45] The temperature dependence of device parameters particularly, V_{OC} vs T provides insight into the dominant recombination processes and effect of defect/trap level that lowers V_{OC}. **Figure 2** depicts temperature dependency of V_{OC} of fresh and degraded devices. These trends are in good agreement with other reports.[46–50] The activation energy (E_A) of the dominant recombination can be estimated by linear extrapolation of V_{OC}-T plots to 0 K as given by equation[43]

$$V_{OC} = \frac{E_A}{q} - \frac{A\,k_B T}{q} \times \ln\left(\frac{J_{00}}{J_{ph}}\right) \qquad (2)$$

where J_{00} and J_{ph} denote reverse saturation current prefactor and constant photocurrent, respectively. J_{00} depends on specific recombination mechanism that dominates reverse saturation current (J_0). The value of E_A was estimated to be ~1.4 eV for fresh device whereas that of the degraded device was found to be ~0.98 eV as depicted in **Fig. 2 (a, b).** Note that the depression of E_A with respect to E_g (E_g-E_A) reflects the strength of recombination at the interfacial defects induced in the perovskite layer.[43,47,51] A noticeable depression of E_A for degraded device indicates strong interface recombination. The deterioration of the interfacial perovskite could be caused by ion migration[28] or formation of voids in CTLs and detachment of interfacial layer.[22] Moreover, **Fig. 2a** reveals a slight deviation of V_{OC} from increasing linear trend below 263 K which could be due to pinning interface, defect in perovskite layer or being contact limited at low temperature.[50] The temperature dependent figures of merit for fresh and aged perovskite devices (**Fig. S6**) also reflect the deterioration trend with decreasing temperature. Particularly, J_{SC} shows a dominant decrease with temperature for degraded device. This must be correlated to either increasing recombination activities or interfacial deterioration with aging.[22,27,33] Note that despite some fluctuations in values, FF and R_S, show no noticeable change in trend with temperature for both fresh and aged devices. Importantly, a decreasing trend of PCE and V_{OC} of devices with decrease in E_A (**Fig. 2c, d**) corroborates that the defect-mediated recombination at the interface significantly affects the device degradation with aging.

This could be due to either of self-degradation of CTLs or worsening of interface or perovskite layer caused by chemical reaction or intrinsic instability of material.[27,33,38] Thus, this result suggests that a robust CTL having superior moisture stability and resistive to ion diffusion can improve the device stability.

3.2. Admittance spectroscopy and instability impact

Admittance spectroscopy (AS) is commonly employed to extract the carrier profile, distribution of defect density and energetic position of the defects within the band gap by tracking the capacitance response from absorber layer.[51,52] Through AS technique, the degradation phenomena are further elucidated. We analyzed the capacitance voltage (C-V) scans of devices as depicted in **Fig. 3**. The Mott-Schottky plot (**Fig. 3a**) shows a full depletion in well confined p-i-n junction. Note that the curve is independent of voltage until the forward bias voltage is close to diffusion potential (V_D)[43] for p-i-n type device. Although a fully depleted perovskite layer between CTLs is retained well in both fresh and degraded devices,[43,53] the diffusion potential (V_D)[43] decreased from ~0.78 to 0.62 V under degradation. This result is analogous to the decreasing trend of V_{OC} with aging (**Table 1, Fig. S2**). Guerrero et al.[28] also observed a similar trend for degraded devices. The decrease in V_D for degraded device suggests that the energetic properties at the interface between the perovskite and contact electrode been modified as a consequence of accumulation of spurious charges at interface with aging.[28] Moreover, although there is no distinct difference in the space charge carrier profile of fresh and degraded device with minimum carrier density in the range of $10^{15}cm^{-3}$ as depicted in **Fig. 3b,** the space charge region (SCR) width was found to be slightly increased by ~10 nm (from ~301 nm for fresh to ~311 nm) for degraded device. An increment in SCR width may be the consequence of diffusion of atomic constituents of perovskite material to the interfacial CTLs due to dissociation or ionic migration with aging.[27,33,54–56] We speculate that the increase

in SCR could be associated with defective interface which dominates the recombination at interface as discussed in the preceding section.

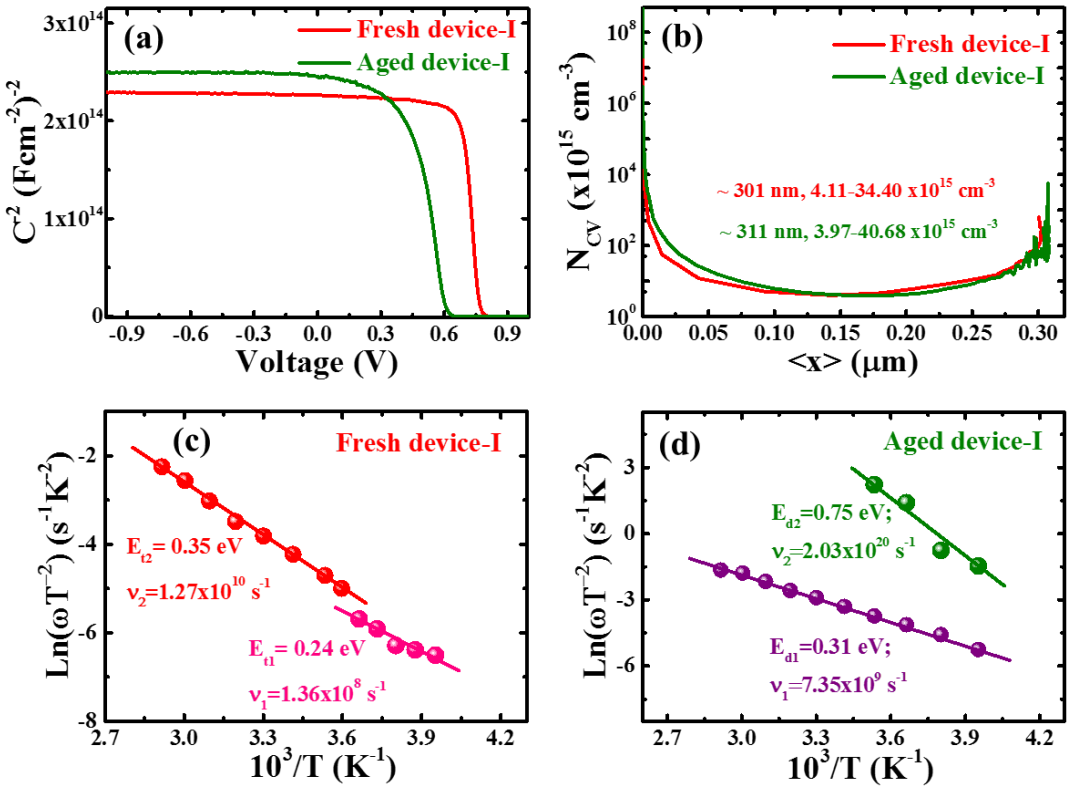

Fig. 3. Admittance spectroscopy of fresh and aged devices; Mott-Schottky plots (a) and SCR carrier density profiles (b) obtained from capacitance voltage (C-V) characteristics of fresh and degraded PSCs. The values in the plots (b) are SCR width, the minimum carrier density and carrier density close to SCR width at zero bias. The estimation of defect levels from Arrhenius plots of fresh (c) and aged (degraded) (d) devices extracted from thermal capacitance frequency (C-f-T) characteristics.

To probe the impact of defect states and defect profile in device with aging, the perovskite devices were investigated by analysing the temperature dependent capacitance-frequency (C-f-T) spectra of fresh and aged devices as depicted in **Fig. S7.** Note that the C-f-T spectra of degraded PSCs revealed a wider variation of capacitance with temperature and distortion in high frequency range. This indicates a higher defect activities induced in device with aging.

The dielectric constant was found to be slightly increased from ~21 to 25 for fresh and degraded device-I which is in the range of reported values.[46,53,57,58] The increase in dielectric constant could be due to increase in ionic accumulation or polarization at interfacial junctions in aged device.[38,57,59] The defect states in devices were calculated from Arrhenius plots (**Fig. 3c, d**) extracted from characteristics C-f-T spectra of devices using the relation,[51]

$$\omega_0 = 2\upsilon_0 T^2 e^{-E_t/k_B T} \quad (3)$$

where υ_0 is emission factor comprising all the temperature independent parameters and E_t is defect energy level. The fresh device-I (**Fig. 3c**) demonstrated two defect states at E_{t1}~0.24 eV (υ_1~1.36× 10^8 s^{-1}) and E_{t2}~0.35 eV (υ_2~1.27× 10^{10} s^{-1}) with emission factors (ν) in respective parentheses whereas the degraded device-I (**Fig. 3d**) revealed deeper trap levels at E_{d1}~0.31 eV and E_{d2}~0.75 eV with emission factors; υ_{d1}~7.35× 10^9 s^{-1} and υ_2~2.03× 10^{20} s^{-1}, respectively. To have further confirmation, we also analyzed the C-f-T spectra of additional devices (degraded). Some of these are depicted in **Fig. S8.** Both fresh and aged devices showed two defect states which are analogous to the reports.[60,61] Indeed, the aged perovskite devices revealed deeper defect states compared to fresh devices (**Fig. S9**). This may be as a consequence of ion migration[27,62] which indicates intrinsic instability of perovskite. Furthermore, although deep defect levels have been induced in degraded perovskite devices, the integrated defect densities of fresh device (~10^{17} cm^{-3}) were found to be one order higher than those of degraded devices (~10^{16} cm^{-3}) for both devices which are in the range of reported values by other groups.[60,61,63–66] The lower defect densities for deep defect states in our degraded devices are close to the report by Heo et al.[60] They estimated integrated defect densities in the range of 10^{14}-10^{15} cm^{-3} for deep defect levels, which is comparatively lower than our estimation. It suggests that the deep defect levels are worse enough to deteriorate device performances even if the degraded devices have lower defect densities.

Furthermore, it is crucial to identify the defect to unveil the reason behind the origin of deep defect states with aging. Though the identification of defect type is rather complicated, following the density functional theory (DFT) calculation,[36–38,67] the shallow defect states in device are attributed to either of iodine vacancy or interstitials (V_I or I_i), methylammonium vacancy (V_{MA}) and lead vacancy (V_{Pb}) whereas the deep defect states in degraded device could be assigned to antisites either of I_{MA} and I_{Pb}. The experimental and theoretical studies indicate that the ionic species (Pb^+, MA^+,I^-) formed by dissociation of $MAPb(I,Cl)_3$ drift within perovskite layer.[27,33,36–38,59,68] Then, unbalanced kinetics of ionic species/constituent atoms induce the deep defects as well as accelerate the chemical reaction between ions (especially most mobile ions I^-) to CTLs and contact electrode.[27,33,38,59,68] Since the defect in perovskite layer impacts on the electron-hole diffusion length and V_{OC} of device,[36] deep defects induced in the degraded device effectively act as SRH nonradiative recombination centers, which contribute for lowering V_{OC} with aging. Therefore, the intrinsic stability of perovskite layer with aging is one of the crucial prerequisites to increase the durability of perovskite device.

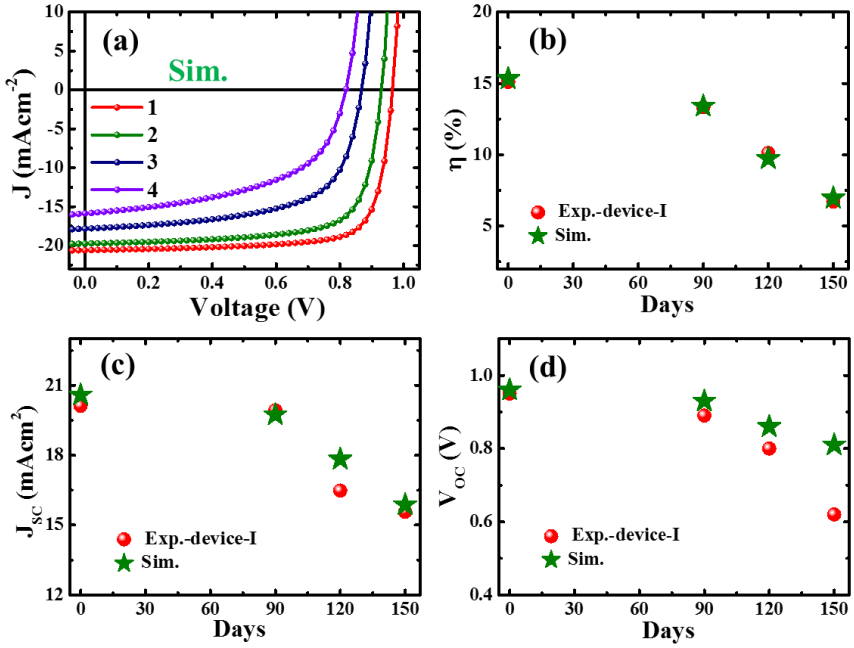

Fig. 4. Current density-voltage (J-V) characteristics from simulation adopting the experimental degradation trend of perovskite devices (a) and the simulation parameters and corresponding

device parameters (numbered 1-4) are as summarized in **Table S3 (supporting information).** The comparative plots of the performance parameters of device-I with the simulated data (b-d).

3.3. Degradation phenomena and simulation

To illustrate the degradation driven by deterioration of interface layer and formation of deep defect with aging, we performed a device simulation using the program SCAPS (ver. 3.3.03),[69] solar cell capacitance simulator adopting the device layers shown in **Fig. S10** imitating the real device with the layer properties (**Table S2**) adopted from our earlier reports.[6,47] Regarding the degradation phenomena, the interfacial deterioration was accounted for by the interface defect density at the interface of CTLs and perovskite layer whereas degradation of perovskite layer was assigned by considering the defect states and defect densities. The simulation results (**Fig. S11)** reveal that the deep defect states and increase in defect density in perovskite and defective interfacial layer have dominant impact on device performance. Some trial simulations have been performed (**Fig. 4a**), which reproduce the basic characteristics of the experimental J-V results (**Fig. 1**). A set of simulation conditions and simulated device parameters are summarized in **Table S3**. An attempt to obtain better fitting without full understanding of the device degradation would be not useful at this stage. Nonetheless, the trend of experimental and simulated device parameters (**Fig. 4b-4d)** lies within an acceptable range. It indicates that the degradation of perovskite device is attributed to the collective consequence of gradual worsening of both interface quality and perovskite layer.

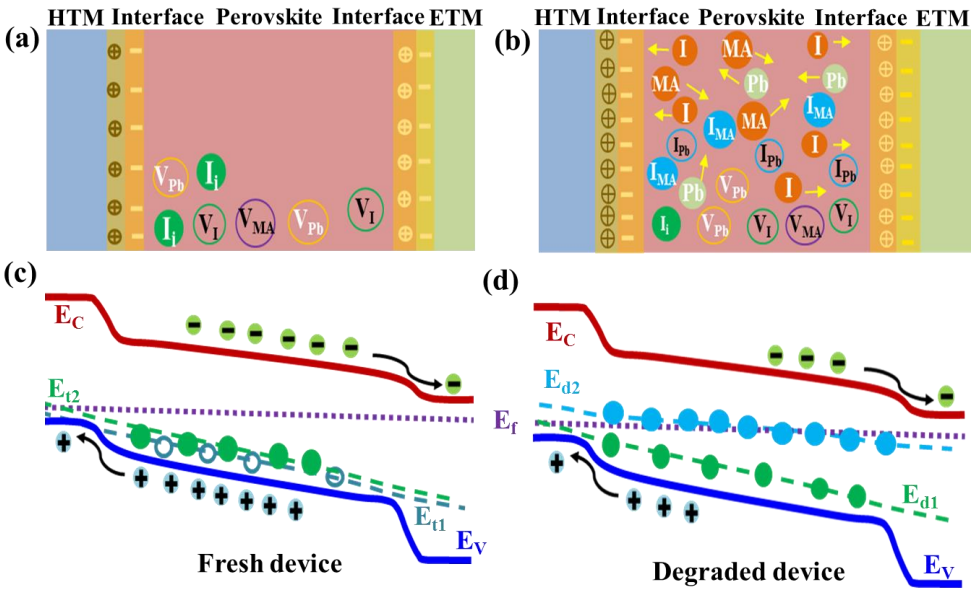

Fig. 5. Schematic diagrams showing the degradation phenomena of encapsulated perovskite device driven by deep defects and interfacial deterioration due to ionic migration and dissociation in fresh (a) and degraded (b) perovskite device and energy band diagram with defect state localization (c, d) respectively. Here atomic constituents with arrow heads represent ionic movements in perovskite layer and towards the interfacial layers. Here, E_C, E_V and E_f stand for energy level of conduction band, valence band, Fermi level in energy band of device and E_{t1}. E_{t2}, E_{d1}, and E_{d2} denote the energetic defect states with in the perovskite layer induced in fresh and degraded device. The filled and empty symbols represent the different types of defect species in perovskite layer.

In the schematic diagrams in **Fig. 5**, we propose the illustration of the degradation phenomena of encapsulated perovskite device induced by deep defects due to ionic migration and dissociation of constituents with aging as discussed above. As shown in **Fig. 5a, b,** the fresh perovskite device is supposed to have intrinsic defects (I_i, V_{Pb}, V_I, V_{MA}) having shallow energetic states[36,38] with accumulation of detrimental charges at interfaces which hamper the carrier dynamics.[38] The vacancy defects, most mobile species in $MAPb(I,Cl)_3$ material, I-related defects and ions formed by dissociation of perovskite are assumed to interact to the interfacial layer dominantly.[27,33,36–38,55,66,67,70] As perovskite layer suffered from gradual

dissociation of atomic constituents and ionic migration to either of CTLs with aging as depicted in **Fig. 5b**, there is formation of deep defects (I_{MA}, I_{Pb}) (**Fig. 5d**) in addition to shallow defects pre-existed in fresh device (**Fig. 5c**) and increases the accumulation or interaction of detrimental charges at either of interfaces leading to degradation of perovskite layer and deterioration of interface layer. This lowers device performance. Obviously, there is still much room to uncover the facts behind the intrinsic instability of perovskite device not only due to ambient atmosphere but also due to internal phenomena and passivation of those detrimental effects to overcome the degradation issue.

4. Conclusions

We have explored the degradation of encapsulated perovskite devices by optoelectronic approach. The correlation of degradation and optoelectronic properties was investigated by analysing the J-V characteristics and capacitance spectra of devices. The degradation of device performances was found to be influenced by deterioration of interfacial layers coupled with traps assisted recombination. The admittance spectroscopy revealed deeper defect levels in perovskite layer and reduction in diffusion potential of the devices, which are believed to be the cause of decrease in open circuit voltage of the device with aging. It is clear that the control of defects in perovskite material and deterioration of CTLs is crucial even for encapsulated perovskite devices to get long term stability.

Associated content

Supporting information

The Supporting Information is available free of charge. Experimental details and characterization, schematic of device structure, plots and table of degraded device parameters,

EDE data, J-V characteristics encapsulated devices under humidity, J-V characteristics under temperature, admittance spectra of fresh and degraded devices, device simulated data and plots.

Notes

The authors declare no competing financial interest.

Acknowledgements

The authors acknowledge the support under the MEXT Program for Development of Environment Technology using Nanotechnology (GREEN), JSPS KAKENHI grant number JP16K06285.

References

1 M. A. Green, K. Emery, Y. Hishikawa, W. Warta, E. D. Dunlop, D. H. Levi and A. W. Y. Ho-baillie, *Prog. Photovolt Res. Appl.*, 2017, **25**, 3–13.

2 A. Kojima, K. Teshima, Y. Shirai and T. Miyasaka, *J. Am. Chem. Soc.*, 2009, **131**, 6050–6051.

3 M. Saliba, T. Matsui, J.-Y. Seo, K. Domanski, J.-P. Correa-Baena, M. K. Nazeeruddin, S. M. Zakeeruddin, W. Tress, A. Abate, A. Hagfeldt and M. Grätzel, *Energy Environ. Sci.*, 2016, **9**, 1989–1997.

4 N. J. Jeon, J. H. Noh, Y. C. Kim, W. S. Yang, S. Ryu and S. Il Seok, *Nat. Mater.*, 2014, **13**, 897–903.

5 C. Bi, Q. Wang, Y. Shao, Y. Yuan, Z. Xiao and J. Huang, *Nat. Commun.*, 2015, **6**, 7747.

6 D. B. Khadka, Y. Shirai, M. Yanagida, T. Masuda and K. Miyano, *Sustain. Energy Fuels*, 2017, **1**, 755–766.

7 S. Shi, Y. Li and H. Wang, *Mater. Horizons*, 2015, **2**, 378–405.

8 J. You, L. Meng, T.-B. Song, T.-F. Guo, Y. (Michael) Yang, W.-H. Chang, Z. Hong, H. Chen, H. Zhou, Q. Chen, Y. Liu, N. De Marco and Y. Yang, *Nat. Nanotechnol.*, 2016,

11, 75–82.

9 C. Chueh, C. Li and A. K. Jen, *Energy Environ. Sci.*, 2015, **8**, 1160–1189.

10 Y. Hou, W. Chen, D. Baran, T. Stubhan, N. A. Luechinger, B. Hartmeier, M. Richter, J. Min, S. Chen, C. Omar, R. Quiroz, N. Li, H. Zhang, T. Heumueller, G. J. Matt, A. Osvet, K. Forberich, Z. Zhang, Y. Li, B. Winter, P. Schweizer, E. Spiecker and C. J. Brabec, *Adv. Mater.*, 2016, **28**, 5112–5120.

11 Y. Deng, Q. Dong, C. Bi, Y. Yuan and J. Huang, *Adv. Energy Mater.*, 2016, 1600372.

12 H. Kim, C.-R. Lee, J. Im, K. Lee, T. Moehl, A. Marchioro, S. Moon, R. Humphry-Baker, J. Yum, J. E. Moser, M. Grätzel and N.-G. Park, *Sci. Rep.*, 2012, **2**, 591.

13 J. H. Noh, S. H. Im, J. H. Heo, T. N. Mandal and S. Il Seok, *Nano Lett.*, 2013, **13**, 1764–1769.

14 W. Chen, Y. Wu, Y. Yue, J. Liu, W. Zhang, X. Yang, H. Chen, E. Bi, I. Ashraful, M. Grätzel and L. Han, *Science (80-.).*, 2015, **350**, 944–948.

15 T. A. Berhe, W.-N. Su, C.-H. Chen, C.-J. Pan, J.-H. Cheng, H.-M. Chen, M.-C. Tsai, L.-Y. Chen, A. A. Dubale and B.-J. Hwang, *Energy Environ. Sci.*, 2016, **9**, 323–356.

16 H. Tsai, W. Nie, J.-C. Blancon, C. C. Stoumpos, R. Asadpour, B. Harutyunyan, A. J. Neukirch, R. Verduzco, J. J. Crochet, S. Tretiak, L. Pedesseau, J. Even, M. A. Alam, G. Gupta, J. Lou, P. M. Ajayan, M. J. Bedzyk, M. G. Kanatzidis and A. D. Mohite, *Nature*, 2016, **536**, 312–316.

17 Z. Wang, Q. Lin, F. P. Chmiel, N. Sakai, L. M. Herz and H. J. Snaith, *Nat. Energy*, 2017, **2**, 17135.

18 G. Grancini, I. Zimmermann, E. Mosconi, D. Martineau and S. Narbey, *Nat Commun*, 2017, **8**, 15684.

19 A. Mei, X. Li, L. Liu, Z. Ku, T. Liu, Y. Rong and M. Xu, *Science (80-.).*, 2014, **345**, 323–356.

20 S. N. Habisreutinger, T. Leijtens, G. E. Eperon, S. D. Stranks, R. J. Nicholas and H. J. Snaith, *Nano Lett.*, 2014, **14**, 5561–5568.

21 D. Wang, M. Wright, N. K. Elumalai and A. Uddin, *Sol. Energy Mater. Sol. Cells*, 2016, **147**, 255–275.

22 Y. Han, S. Meyer, Y. Dkhissi, K. Weber, J. M. Pringle, U. Bach, L. Spiccia and Y.-B. Cheng, *J. Mater. Chem. A*, 2015, **3**, 8139–8147.

23 S. Lee, S. Kim, S. Bae, K. Cho, T. Chung, L. E. Mundt, S. Lee, S. Park, H. Park, M. C. Schubert, S. W. Glunz, Y. Ko, Y. Jun, Y. Kang, H. Lee and D. Kim, *Sci. Rep.*, 2016, **6**, 38150.

24 T. Leijtens, G. E. Eperon, S. Pathak, A. Abate, M. M. Lee and H. J. Snaith, *Nat. Commun.*, 2013.

25 J. M. Frost, K. T. Butler, F. Brivio, C. H. Hendon, M. Van Schilfgaarde and A. Walsh, *Nano Lett.*, 2014, **14**, 2584−2590.

26 G. Niu, X. Guo and L. Wang, *J. Mater. Chem. A*, 2015, **3**, 8970–8980.

27 T. Zhang, X. Meng, Y. Bai, S. Xiao, C. Hu, Y. Yang, H. Chen and S. Yang, *J. Mater. Chem. A*, 2017, **5**, 1103–1111.

28 A. Guerrero, J. You, C. Aranda, Y. S. Kang, H. Zhou, J. Bisquert and Y. Yang, *ACS Nano 2016*, 2016, **10**, 218−224.

29 S. de Wolf, J. Holovsky, S.-J. Moon, P. Löper, B. Niesen, M. Ledinsky, F. Haug, J. Yum and C. Ballif, *J. Phys. Chem. C*, 2014, **5**, 1035–139.

30 A. M. A. Leguy, Y. Hu, M. Campoy-Quiles, M. I. Alonso, O. J. Weber, P. Azarhoosh, M. Van Schilfgaarde, M. T. Weller, T. Bein, J. Nelson, P. Docampo and P. R. F. Barnes, *Chem. Mater.*, 2015, **27**, 3397–3407.

31 J. Yang, B. D. Siempelkamp, D. Liu and T. L. Kelly, *ACS Nano*, 2015, **9**, 1955–1963.

32 N. Ahn, K. Kwak, M. S. Jang, H. Yoon, B. Y. Lee, J. Lee, P. V Pikhitsa, J. Byun and M.

Choi, *Nat. Commun.*, 2016, **7**, 13422.

33 D. Bryant, N. Aristidou, S. Pont, I. Sanchez-Molina, T. Chotchunangatchaval, S. Wheeler, J. R. Durrant and S. A. Haque, *Energy Environ. Sci.*, 2016, **9**, 1655–1660.

34 D. Song, J. Ji, Y. Li, G. Li, M. Li, T. Wang, D. Wei, P. Cui, Y. He and J. M. Mbengue, *Appl. Phys. Lett.*, 2016, **108**, 93901.

35 W.-J. Yin, J.-H. Yang, J. Kang, Y. Yan and S.-H. Wei, *J. Mater. Chem. A*, 2015, **3**, 8926–8942.

36 A. Buin, P. Pietsch, J. Xu, O. Voznyy, A. H. Ip, R. Comin and E. H. Sargent, *Nano Lett.*, 2014, **14**, 6281−6286.

37 J. M. Azpiroz, E. Mosconi, J. Bisquert and F. De Angelis, *Energy Environ. Sci.*, 2015, **8**, 2118–2127.

38 W. S. Yang, J. H. Noh, N. J. Jeon, Y. C. Kim, S. Ryu, J. Seo and S. Il Seok, *Science (80-.).*, 2015, **348**, 1234–1237.

39 C. Z. Li, C. C. Chueh, F. Ding, H. L. Yip, P. W. Liang, X. Li and A. K. Y. Jen, *Adv. Mater.*, 2013, **25**, 4425–4430.

40 C. Besleaga, L. E. Abramiuc, V. Stancu, A. G. Tomulescu, M. Sima, L. Trinca, N. Plugaru, L. Pintilie, G. A. Nemnes, M. Iliescu, H. Gud, A. Manolescu and I. Pintilie, *J. Phys. Chem. Lett.*, 2016, **7**, 5168−5175.

41 V. Nadenau, U. Rau, A. Jasenek and H. Schock, *J. Appl. Phys.*, 2000, **87**, 584.

42 D. B. Khadka, S. Kim and J. Kim, *J. Phys. Chem. C*, 2016, **120**, 4251–4258.

43 S. S. Hegedus and W. N. Shafarman, *Prog. Photovoltaics Res. Appl.*, 2004, **12**, 155–176.

44 A. Nakane, H. Tampo, M. Tamakoshi, S. Fujimoto, K. M. Kim, S. Kim, H. Shibata, S. Niki and H. Fujiwara, *J. Appl. Phys.*, 2016, **120**, 64505.

45 A. Poglitsch and D. Weber, *J. Chem. Phys.*, 1987, **87**, 6373–6378.

46 S. Chen, Y. Hou, H. Chen, M. Richter, F. Guo, S. Kahmann, X. Tang, T. Stubhan, H. Zhang, N. Li, N. Gasparini, C. O. R. Quiroz, L. S. Khanzada, G. J. Matt, A. Osvet and C. J. Brabec, *Adv. Energy Mater.*, 2016, 1600132.

47 D. B. Khadka, Y. Shirai, M. Yanagida, J. W. Ryan and K. Miyano, *J. Mater. Chem. C*, 2017, **5**, 8819–8827.

48 L. Cojocaru, S. Uchida, Y. Sanehira, G.-P. Victoria, B. Juan, N. Jotaro, K. Takaya and H. Segawa, *Chem. Lett.*, 2015, **44**, 1557–1559.

49 H. Zhang, X. Qiao, Y. Shen, T. Moehl, S. M. Zakeeruddin and M. Wang, *J. Mater. Chem. A*, 2015, **3**, 11762–11767.

50 W. L. Leong, Z. Ooi, D. Sabba, C. Yi, S. M. Zakeeruddin, M. Graetzel, J. M. Gordon, E. A. Katz and N. Mathews, *Adv. Mater.*, 2016, **28**, 2439–2445.

51 D. Abou-Ras, T. Kirchartz and U. Rau, *Advanced Characterization Techniques for Thin Film Solar Cells*, Wiley-VCH Verlag GmbH & Co. KGaA: Weinheim, Germany, 2016.

52 D. B. Khadka, S. Kim and J. Kim, *J. Phys. Chem. C*, 2015, **119**, 12226–12235.

53 O. Almora, C. Aranda, E. Mas-Marz and G. Garcia-Belmonte, *Appl. Phys. Lett.*, 2016, **109**, 173903.

54 H. Lee, S. Gaiaschi, P. Chapon, A. Marronnier, H. Lee, J.-C. Vanel, D. Tondelier, J.-E. Bourée, Y. Bonnassieux and B. Geffroy, *ACS Energy Lett.*, 2017, **2**, 943–949.

55 Y. Yuan and J. Huang, *Acc. Chem. Res.*, 2016, **49**, 286–293.

56 S. Kim, S. Bae, S.-W. Lee, K. Cho, K. D. Lee, H. Kim, S. Park, G. Kwon, S.-W. Ahn, H.-M. Lee, Y. Kang, H.-S. Lee and D. Kim, *Sci. Rep.*, 2017, **7**, 1200.

57 I. Zarazua, J. Bisquert and G. Garcia-Belmonte, *J. Phys. Chem. Lett.*, 2016, **7**, 525–528.

58 O. Almora, I. Zarazua, E. Mas-marza, I. Mora-sero, J. Bisquert and G. Garcia-belmonte, *J. Phys. Chem. Lett.*, 2015, **6**, 1645−1652.

59 R. Cao, F. Xu, J. Zhu, S. Ge, W. Wang, H. Xu, R. Xu, Y. Wu, Z. Ma, F. Hong and Z.

Jiang, *Adv. Energy Mater.*, 2016, 1600814.

60 S. Heo, G. Seo, Y. H. Lee, D. Lee, M. Seol, J. Lee, J.-B. Park, K. Kim, D.-J. Yun, Y. Kim, J. Shin, T. K. Ahn and M. K. Nazeeruddin, *Energy Environ. Sci.*, 2017, 0–6.

61 M. Samiee, S. Konduri, B. Ganapathy, R. Kottokkaran, H. A. Abbas, A. Kitahara, P. Joshi, L. Zhang, M. Noack and V. Dalal, *Appl. Phys. Lett.*, 2014, **105**, 153502.

62 J. M. Azpiroz, E. Mosconi, J. Bisquert and F. De Angelis, *Energy Environ. Sci.*, 2015, **8**, 2118–2127.

63 H. Duan, H. Zhou, Q. Chen, P. Sun, S. Luo, T. Song, B. Bob and Y. Yang, *Phys. Chem. Chem. Phys.*, 2015, **17**, 112–116.

64 J. H. Heo, D. H. Song, H. J. Han, S. Y. Kim, J. H. Kim, D. Kim, H. W. Shin, T. K. Ahn, C. Wolf, T. W. Lee and S. H. Im, *Adv. Mater.*, 2015, **27**, 3424–3430.

65 M. Jiang, F. Lan, B. Zhao, Q. Tao, J. Wu, D. Gao and G. Li, *Appl. Phys. Lett.*, 2016, **108**, 1–5.

66 Y. Shao, Z. Xiao, C. Bi, Y. Yuan and J. Huang, *Nat. Commun.*, 2014, **5**, 5784.

67 M. H. Du, *J. Mater. Chem. A*, 2014, **2**, 9091–9098.

68 K. Miyano, M. Yanagida, N. Tripathi and Y. Shirai, *J. Phys. Chem. Lett.*, 2016, **7**, 2240−2245.

69 M. Burgelman, P. Nollet and S. Degrave, *Thin Solid Films*, 2000, **361**, 527–532.

70 V. V Brus, F. Lang, J. Bundesmann, S. Seidel, A. Denker, B. Rech, G. Landi, H. C. Neitzert, J. Rappich and N. H. Nickel, *Adv. Electron. Mater.*, 2017, 1600438.

Table of Contents Graphics

The degradation of performance perovskite device is found to be driven by deterioration interface in device and induced deep trap assisted recombination in the perovskite with aging.